RSC Advances

RSC Publishing

PAPER

Molecular and continuum hydrodynamics in graphene nanopores†

Cite this: *RSC Advances*, 2013, **3**, 9365

M. E. Suk and N. R. Aluru*

Received 6th February 2013,
Accepted 19th April 2013

DOI: 10.1039/c3ra40661j

www.rsc.org/advances

An ultrathin graphene membrane is a promising candidate for various applications such as gas separation, water purification, biosensors, *etc*. In this study, we investigate water transport mechanisms and hydrodynamic properties such as water flux, pressure variation, velocity, viscosity, slip length, *etc*. Due to the unique water structure, confined in the radial direction and layered in the axial direction of the pore, water viscosity and slip length increase with a decrease in the pore radius, in contrast to water confined in a carbon nanotube. As the diameter of the pore increases, the water transport mechanism transitions from collective diffusion to frictional flow described by the modified Hagen–Poiseuille equation. Graphene membrane is shown to be ultra-efficient by comparing the permeation coefficient of graphene membrane to that of a carbon nanotube and an ultrathin silicon membrane. We envision that the study presented here will help to understand and design various membrane separation processes using graphene membrane.

1. Introduction

Advances in fabrication, measurement and characterization have led to intense research in the area of nanoporous membranes.[1] High performance membranes, that can exhibit superior selectivity and high flux, can find numerous applications. For example, efficient water filtration and desalination can reduce energy consumption, which can have a positive effect on both the water shortage problem[2,3] and the growing energy crisis.[4] Nanoporous membranes that are selectively transporting ions or delivering biomolecules such as DNA, can lead to further advances in biological research and assist in the development of lab-on-a-chip devices or biosensors.[1,5] Gas separations, including hydrogen and carbon dioxide separation, using nanoporous membranes can enable advances in clean energy technology.[6] These and many other applications can benefit from advances in novel and energy efficient nanoporous membranes.

Recently, carbon nanotubes (CNT) have gained significant interest as nanoporous membranes as they have been shown to be efficient for mass transport due to smooth and hydrophobic surface.[7] It was shown that water flow rate through a CNT membrane is three to four orders of magnitude higher compared to that from the no-slip Hagen–Poiseuille's (HP) equation.[8,9] Molecular dynamics (MD) simulations have shown a large amount of liquid slip at the nanotube surface, representing low frictional resistance.[10,11] Recently, silicon-based membranes were fabricated with a membrane thickness of 15 nm[12,13] to increase the efficiency by reducing the membrane length. Even though silicon-based membranes did not show the dominant liquid slip at the surface[13] due to the hydrophilic nature of the surface, flow rate through these membranes were higher compared to that through thicker membranes made of a silica–surfactant nanocomposite[12] or CNT.[13]

Owing to its ultra-small thickness, nanoporous graphene membranes are promising candidates for various applications. Since the graphene membrane is only a single-atom thick, it can be considered as the thinnest membrane possible. Nanopores of various diameters can be realized in graphene by irradiation with an electron beam.[14] Nanopores in graphene are known to be stable over time despite the extreme thinness of graphene.[15] Due to its robustness and potential, nanoporous graphene has been suggested for DNA sequencing.[15–17] In addition, various applications such as ion and gas separation have also been proposed.[18,19]

Understanding water transport mechanisms and hydrodynamic properties in membranes is essential to characterize and design membranes for various applications mentioned above. In nanopores, water transport mechanisms can differ from the continuum hydrodynamics description and water properties under confinement can be different from the bulk values. Numerous theoretical and experimental studies have

Department of Mechanical Science and Engineering, Beckman Institute for Advanced Science and Technology, University of Illinois at Urbana-Champaign, Urbana, Illinois 61801, USA. E-mail: aluru@illinois.edu

† Electronic supplementary information (ESI) available: Water velocity profile in the axial direction. No-slip hydrodynamics by Dagan *et al.* Calculation of viscosity and slip length using NEMD and Green-Kubo relation. Definition of pore radius and length. Calculation of diffusion coefficient and collective diffusion coefficient. Effect of thermal motion of graphene membrane. See DOI: 10.1039/c3ra40661j

been performed to understand structure, dynamics and transport of water confined in CNTs[8–11] and in graphene slabs.[20,21] However, very little is known regarding water transport through graphene nanopores despite their promising characteristics. Hydrodynamics and frictional losses can be quite different in graphene membranes compared to thicker membranes and these need to be understood in great detail to realize the full potential of graphene nanopores. In this paper, we perform detailed studies to understand water transport mechanisms and hydrodynamic properties of water in various diameter graphene nanopores.

2. Methods

We performed molecular dynamics (MD) simulations of water flow through graphene nanopores. Fig. 1 shows the simulation setup and water-filled graphene nanopores of various diameters. Pore radii we considered in this work are 0.283 nm, 0.424 nm, 0.704 nm, 0.933 nm, 1.169 nm, 1.511 nm and 1.888 nm. Pore radius is determined by measuring the distance from the pore axis to the location where the water density dropped to below 2% of bulk value (see ESI† for determination of the pore radius). Corresponding center-to-center radii calculated by averaging the distance from the pore axis to the center of the carbon atoms in the pore edge are 0.424 nm, 0.526 nm, 0.911 nm, 1.136 nm, 1.374 nm, 1.687 nm and 2.083 nm. Graphene pores are generated by removing atoms whose coordinates satisfy the condition $(x - C_x)^2 + (y - C_y)^2 < R^2$ where C_x and C_y are the x and y coordinates of the pore center, respectively. Pores are not passivated to remove any effect from passivating atoms such as charges and interaction energies.

The carbon atoms of the graphene membrane were modeled as Lennard-Jones spheres with the parameters σ = 0.339 nm and ε = 0.2897 kJ mol^{-1}.[22] Water molecules were modeled using the simple point charge-extended (SPC/E) water model.[23] Both x and y dimensions of the graphene membrane (see Fig. 1) range from about 4 nm to 8 nm in length depending on the pore radius to keep the porosity (pore area/total membrane area) constant. The z dimension of the total system is approximately 12 nm in length. The graphene membrane is centered separating the two water baths. The total number of water molecules varied from 6479 to 24 046, depending on the system size. Periodic boundary condition was applied in all the three-directions. Nosé-Hoover thermostat was used to maintain the temperature at 300 K with a time constant of 0.1 ps. Graphene membranes were kept rigid during the simulation by fixing carbon atoms to their lattice positions. Thermal motion of graphene had negligible effect on results (see ESI†). SETTLE algorithm was used to constrain the angle and bond length of SPC/E water. It is reported that flexible water models produce similar water dynamics in graphene nanopores.[24]

Equation of motion was integrated with a 1 fs time step. The simulation box size in the z direction was adjusted to maintain the system pressure at 1 bar for 1 ns and then an NVT ensemble was run for 1 ns to attain an initial equilibrium configuration. For pressure-driven flow simulation, an external pressure drop was applied using the method proposed by Zhu *et al.*[25] for an additional 10 ~ 20 ns after the equilibration run. Pressure drop was created by applying external forces on the oxygen atoms of the water molecules in the Δz = 1 nm slab region at the end of system.[26] Applied force on an individual water molecule is given by, $f = \Delta PA/n$ where ΔP is the desired pressure drop, A is the area of the membrane and n is the total number of water molecules on which the external force is applied.[25] For the Green-Kubo (GK) calculations, equilibrium MD simulations were run for 5 ns with data sampling every 20 fs. For the calculation of the diffusion coefficient and the collective diffusion coefficient, equilibrium simulation was run for 10 ns with data sampling every 500 fs. All the simulations were performed using Gromacs.[27]

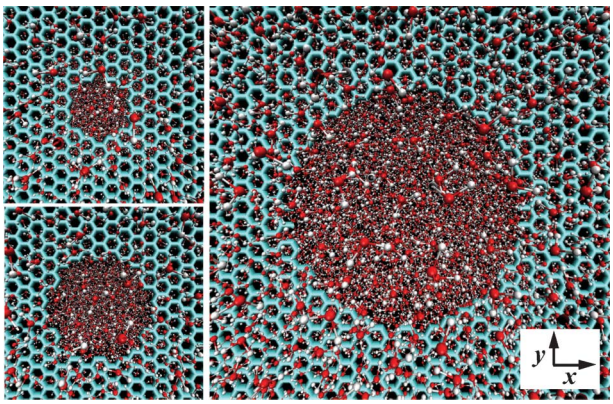

Fig. 1 Visualization of water molecules permeating through graphene nanopores of various radii. Graphene membranes are shown in blue. Water molecules are described by red (oxygen) and white (hydrogen) spheres. Pore radii are R = 0.424 nm (left top) R = 0.933 nm (left bottom) and R = 1.51 nm (right).

3. Results and discussion

3.1 Pressure driven flow

A total pressure drop, ΔP_{total}, varying from 10 MPa to 300 MPa is applied across the graphene membrane. Water flux is measured by counting the number of water molecules transported through the pore during the course of the simulation time and is shown in Fig. 2(b). A linear relation between water flux and the total pressure drop is observed as shown in Fig. 2(b).

We found that the variation of the local pressure normalized by the applied total pressure drop is nearly identical (see Fig. 2(a)) for various pressure drops. This indicates that the entrance and exit pressure loss is proportional to the applied total pressure drop. Thus, water flux is also proportional to the applied total pressure drop as shown in Fig. 2(b). Such flow behavior can be explained by the low Reynolds number creeping flow predicting a linear relation between flow rate and the total pressure drop.[28–30] Although a high pressure

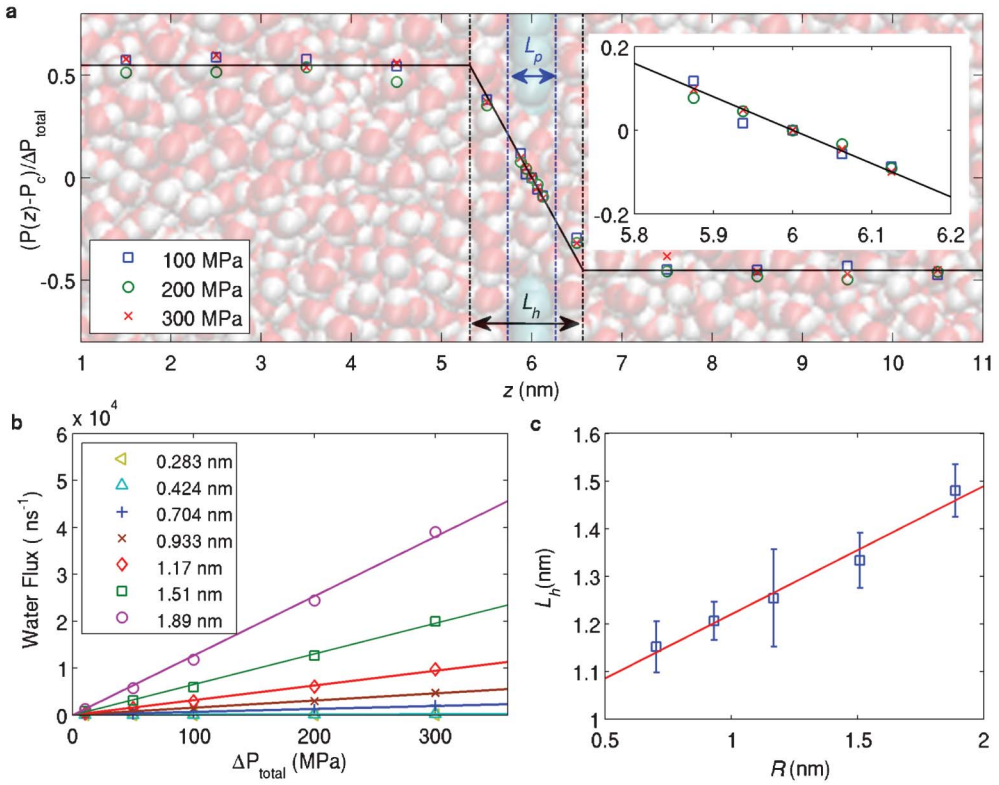

Fig. 2 (a) Pressure distribution normalized by the total applied pressure drop along the flow direction. The three different symbols indicate total applied pressure drops of 100 MPa, 200 MPa and 300 MPa. Normalized pressure distributions are close to each other and are represented by a solid line. Graphene pore length (L_p) and hydrodynamic membrane length (L_h) are graphically depicted. Lp = 0.54 nm and L_h = 1.25 nm for pore radius of 1.169 nm. (Inset) Closer view of linear pressure distribution inside the pore. (b) Water flux through various radii graphene nanopores. Water flux is linear with applied pressure drop. (c) Variation of the hydrodynamic membrane length with graphene pore radius. Hydrodynamic membrane length increases linearly with the pore radius. Solid line is a linear fit of the data.

drop is applied, the Reynolds number is of the order of $0.01 \sim 0.1$ in the present study. Since viscous term is dominant in low Reynolds number flow, Hagen–Poiseuille(HP)'s flow is proposed and corrected in the next section to predict the permeation coefficient of graphene nanopores. The deviations of water properties in graphene nanopores from the bulk properties are also investigated.

3.2 Corrected Hagen–Poiseuille's equation and hydrodynamic membrane length

The flow domain is symmetric and our results indicate that $du/dz = 0$ at the pore center ($z = z_c$) where u is the velocity in the axial direction (see ESI†). Under the assumption, $du/dz = 0$, HP equation can be derived from the mass and momentum conservation equations. Using the HP equation modified by the slip boundary condition, fluid velocity in the radial direction is given by

$$u(r) = \left(-\frac{1}{4\mu} r^2 + \frac{R^2}{4\mu} + \frac{R}{2\mu}\delta \right) \frac{dP}{dz} \qquad (1)$$

where μ is the viscosity, R is the pore radius and δ is the slip length satisfying $\delta = u(R)(du/dr)_{r=R}$ ($r = 0$ is pore center). Although the graphene nanopore region is very thin, an approximately linear pressure drop (see inset of Fig. 2(a)) and a near uniform velocity in the axial direction (see inset of Fig. S1 in ESI†) indicate that the HP equation can be used to obtain good insights into transport through the nanopore. dP/dz is usually obtained by $\Delta P_p/L_p$, by taking into account entrance and exit pressure losses, where L_p is the pore length depicted in Fig. 2(a), and ΔP_p is the pressure drop across the pore length L_p. $\Delta P_p = \Delta P_{total} - \Delta P_{loss}$, where ΔP_{loss} is the pressure loss at the entrance and exit. To simplify calculation of dP/dz, where the total applied pressure drop, ΔP_{total}, is used, we define a hydrodynamic membrane length as, $L_h = \Delta P_{total}/(dP/dz)$. Then, dP/dz can be computed as $\Delta P_{total}/L_h$. L_h is graphically depicted in Fig. 2(a). We note that L_h is independent of the applied pressure drop or fluid velocity, and it effectively takes into account the entrance and exit pressure losses. L_h is obtained using a linear fit to the variation of $P(z)/\Delta P_{total}$ with the axial direction (z) in the pore region (see inset of Fig. 2(a)). Averaged fit is superimposed in the inset of Fig. 2(a) with a solid line.

Since L_h is a geometrical variable, it depends on the pore radius. We repeated the calculation of hydrodynamic length L_h for various pore radii and this is plotted in Fig. 2(c). L_h increases linearly with the pore radius and it is given by the empirical relation

$$L_h = 0.27R + 0.95 \quad (2)$$

The solid line in Fig. 2(c) represents the relation given in eqn (2). For low Reynolds number hydrodynamics, the theory developed by Dagan *et al.*[28] can be used to derive an expression for L_h and we note that L_h depends linearly on the pore radius in Dagan *et al.* theory as well (see ESI†) However, Dagan's equation is developed under the assumption of no-slip boundary condition where the fluid velocity is zero at the wall. Thus, Dagan's equation is not directly applicable for water transport through graphene due to the slip boundary condition.

By introducing L_h, eqn (1) can be modified as,

$$u(r) = \left(-\frac{1}{4\mu} r^2 + \frac{R^2}{4\mu} + \frac{R}{2\mu}\delta \right) \frac{\Delta P_{total}}{L_h} \quad (3)$$

The accuracy of eqn (3)will depend on water properties such as viscosity μ and slip length δ and geometrical variables such as the pore radius R and the hydrodynamic membrane length L_h.

Water transport properties such as viscosity μ and slip length δ can be obtained using non equilibrium MD (NEMD) or equilibrium MD (EMD) simulations. In an NEMD simulation, liquid flow is driven by an external field such as gravity, pressure gradient or shear stress and liquid properties can be calculated by comparing the velocity profile to standard models such as Poiseuille's flow or Couette flow. On the other hand, in an EMD simulation, liquid properties can be obtained by applying Green-Kubo (GK) relations, which are expressed as auto-correlation functions of variables fluctuating at equilibrium. In certain cases, these methods can result in inaccurate liquid properties (see ESI† for more discussion). To obtain accurate water properties, in this work, we investigate both NEMD and EMD simulations and found good agreement as shown in Fig. 3(a) and Fig. 3(b). Detailed calculation procedure on NEMD and EMD method can be found in the ESI.† In addition, calculation of μ and δ can be sensitive to the small change in pore radius R and pore length L_p. Thus, a proper and consistent definition of the pore radius and length is necessary. We defined R and L_p based on water density by finding location where water density dropped below 2%. More discussion on this can be found in the ESI.†

Velocity profile $u(r)$ obtained by substituting μ and δ calculated from the GK relations into eqn (3) is compared to the NEMD pressure-driven flow simulation in Fig. 3(c). Since the agreement is good, we can conclude that water flow through the graphene nanopore can be predicted by the corrected HP equation.

In the next section, the variation of viscosity and slip length with the pore radius is investigated.

3.3 Variation of viscosity and slip length with radius of the graphene nanopore

We investigated the variation of viscosity and slip length with the pore radius and these are shown in Fig. 4(a) and 4(b), respectively. These are obtained using GK relations. Both viscosity and slip length monotonically decrease with the increase in the pore radius. At the limit of infinite pore radius, viscosity should approach the bulk viscosity, μ_{bulk} = 0.00085 Pa·s[31] and the corresponding slip length is $\delta_{R\to\infty}$ = 0.205 nm. $\delta_{R\to\infty}$ is calculated from friction coefficient of a flat graphene nano slit whose separation width is 1.169 nm. This is to capture the case of R → ∞. Since Cieplak *et al.*[32] reported that the slip length is independent of the separation width of the channel, it can be concluded that the degree of curvature mainly contributes to the variation of the friction coefficient with the radius. Variation of μ and δ with the pore radius are given by the empirical relations,

and $$\mu(R) = C_1/R + 0.00085 \text{ Pa s} \quad (4)$$

$$\delta(R) = C_2/R + 0.205 \text{ nm} \quad (5)$$

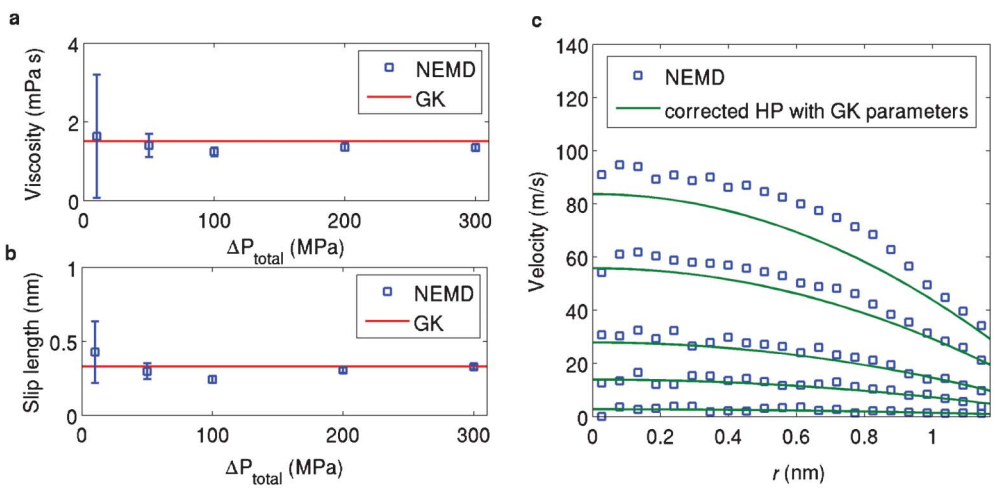

Fig. 3 (a) Viscosity and (b) slip length calculated using NEMD simulations and Green-Kubo (GK) relation. (c) Comparison of velocity profiles from NEMD simulations and corrected HP equation with water properties obtained from the GK relation. In NEMD simulation, velocity profile is calculated by averaging the center-of-mass velocities of individual water molecules located in the cylindrical region centered about the pore axis and the length of cylinder is equal to the carbon diameter. Each line and squared symbol profile represents a different pressure drop, ΔP = 10 MPa, 50 MPa, 100 MPa, 200 MPa and 300 MPa. Data is obtained for R = 1.169 nm pore.

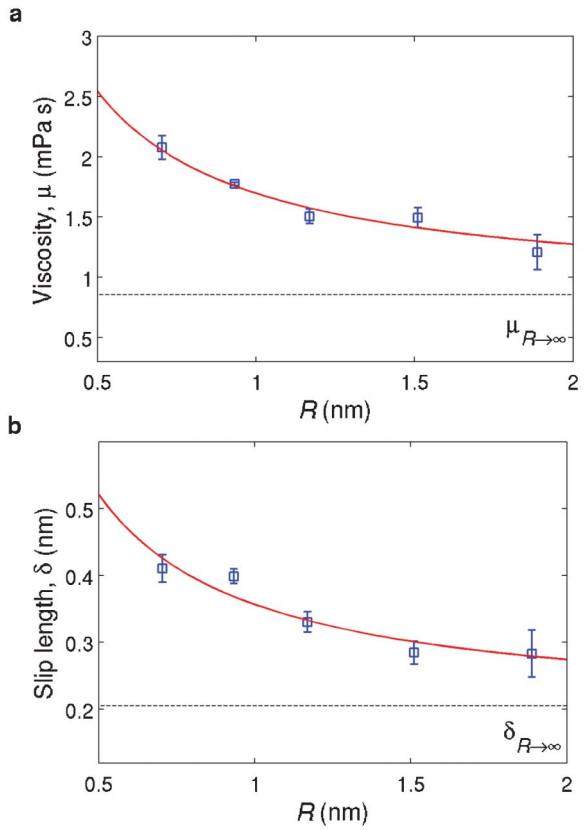

Fig. 4 (a) Viscosity and (b) slip length obtained using GK relations. Solid lines are empirical fits given by eqn (4) and eqn (5). Dashed lines indicate viscosity and slip length when the radius of the pore approaches infinity.

where R is pore radius in nm, and C_1 and C_2 are the unknown coefficients. By using a least-squares method, C_1 and C_2 are determined to be 0.000847 Pa s nm and 0.1517 nm^2, respectively. These relations are plotted in Fig. 4(a) and (b) as a solid line.

Slip length and viscosity of water confined in a graphene nanopore are different from those in a CNT. Slip length of water in a graphene nanopore is significantly smaller compared to that in a CNT. At the water/CNT interface, slip length ranges from several hundreds to tens of thousands of nanometers.[8,9] The viscosity of water confined in a graphene nanopore is higher than that of water confined in a similar diameter CNT.[11,33,34] Variation of water viscosity and slip length with the pore radius in the case of graphene is also different from that of in the infinite CNT. Slip length of water confined in the CNT decreases with the increase in pore radius[11] as $\delta \sim 1/r^3$, while the slip length of water moving outside the CNT increased with the CNT radius.[35] Viscosity of water confined in the CNT increases with the increase in pore radius until it approaches the bulk viscosity.[11,33,34] The increase in viscosity with the decrease in radius in graphene nanopore is related to the water structure, which is discussed in the next section. Due to the statistical inaccuracy, water viscosity and slip length are not measured for R = 0.283 nm and R = 0.424 nm graphene nanopores.

3.4 Density and diffusion coefficient

Water structure along the axial direction in a graphene nanopore is unique and different from that in the interior of the CNT. Layered water structure, described by density oscillations in the radial direction, at the surface of the CNT was reported by various authors.[10,33,36] In the case of graphene nanopore, similar water layering in the radial direction is observed. However, more importantly, the water molecules are also layered in the flow/axial direction (z-direction) as shown in Fig. 5(a) and 5(b). Fig. 5(a) and 5(b) indicate that the degree of density fluctuation increases as the radius of the graphene nanopore decreases. This is due to the increasing influence of graphene atoms on the water molecules. As the pore radius decreases, an increasing fraction of the water molecules are within a distance where the van der Waals interaction between the graphene atoms and the water molecules is significant.

To quantify the water layering effect, we defined the water layering factor as $W_L = (\rho_{max} - \rho_{min})/\rho_{bulk}$ where ρ_{max} and ρ_{min} are the maximum and minimum density near the surface. Water layering factor, W_L, decreases and approaches zero as the pore radius increases. We show that viscosity is related to the water layering effect by noting that viscosity increases linearly with the layering factor, W_L. This is shown in Fig. 5(c). Using linear extrapolation, we also note in Fig. 5(c) that water viscosity approaches the bulk viscosity as W_L approaches zero. One plausible explanation for the increase in water viscosity with the increase in water layering factor is due to the low diffusion of water in the axial direction due to the layered structure. It should be noted that water confined in the CNT[10,11] or in a nano slab configuration[37,38] does not experience the water layering effect in the flow direction as in the case of the graphene nanopore. Thus, the magnitude of viscosity or the variation of viscosity with pore radius in graphene is not consistent with studies on other nanopores.

We calculated the diffusion coefficient in the axial direction to understand the effect of the layered water structure on the water movement. As shown in Fig. 5(d), diffusion coefficient in the graphene nanopore is lower than the bulk diffusion coefficient,[39] $D_z = 2.69 \times 10^{-9}$ m^2 s^{-1}. Furthermore, diffusion coefficient decreases with the decrease in the pore radius. This indicates that diffusion coefficient decreases as the effect of water layering in the axial direction increases. Water immobilization at a critical pore radius, such as the ice-like structure in CNT,[39] is not observed. Water diffusion coefficient for R = 0.283 nm pore is comparable to that for the R = 0.424 nm pore. In the R = 0.283 nm case, single file water molecules[7,26] are observed. In this case, water molecules are highly correlated and diffusion coefficient does not necessarily follow the trend observed for larger pores. Once the variation of the water properties with pore radii are obtained, we calculate the permeation coefficients of graphene nanopores of various radii using the corrected HP equation. These results are compared to the results from pressure driven flow simulation and other experimental data in the following section.

3.5 Permeability of graphene nanopore

Permeation coefficient is defined as $p_Q = Q/\Delta P$, where Q is the volumetric flow rate and ΔP is the applied pressure drop. A

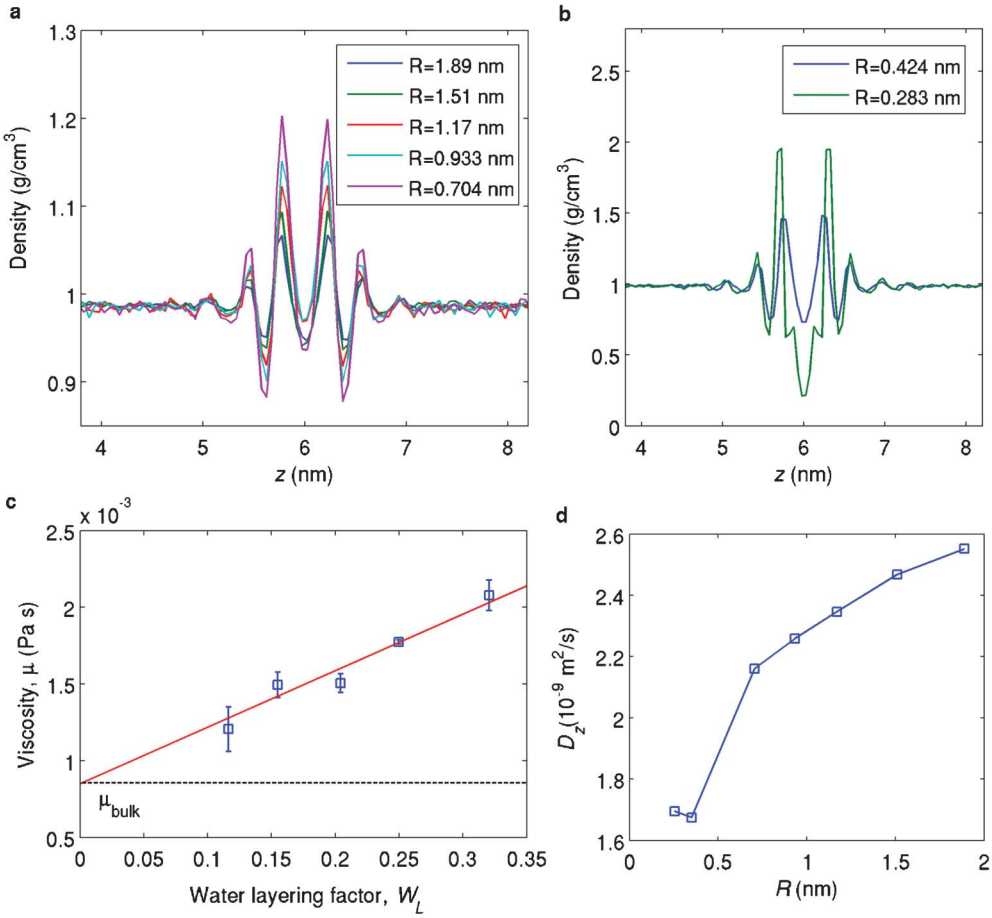

Fig. 5 Water density in the axial direction for (a) radius varying from R = 0.704 nm to R = 1.89 nm and (b) R = 0.283 nm, R = 0.424 nm. z is the axial direction and the graphene membrane is located at z = 6 nm. (c) Relation between water viscosity and water layering factor. A linear fit is shown by the solid line. (d) Variation of the axial diffusion coefficient with pore radius.

higher p_Q indicates a more energy-efficient membrane that delivers more water for a given pressure drop. p_Q can be directly determined from the NEMD pressure-driven flow simulation by a linear fitting of Q (or water flux) *vs.* ΔP relation (see Fig. 2(b)). The permeation coefficient corresponding to graphene nanopores of various diameters is shown in Fig. 6(a).

Permeation coefficient can also be theoretically predicted from the corrected HP relation. By integrating $u(r)$ given by eqn (3), Q can be determined as

$$Q = \frac{\pi(R^4 + 4R^3\delta)}{8\mu}\frac{\Delta P}{L_h} \tag{6}$$

Thus,

$$p_Q(R) = \frac{\pi(R^4 + 4R^3\delta)}{8\mu}\frac{1}{L_h} \tag{7}$$

By substituting the empirical relations for $L_h(R)$, $\mu(R)$ and $\delta(R)$ (eqn (2), (4) and (5)) obtained in this study, we calculated $p_Q(R)$. This is compared to the permeation coefficient obtained from the NEMD simulation in Fig. 6(a). They are in good agreement when the graphene pore radius is larger than 0.484 nm. p_Q calculated from no-slip hydrodynamics is also shown in Fig. 6(a). No-slip hydrodynamics at low Reynolds number is derived by Dagan *et al.*[28] for flow through a circular pore. We substituted a graphene pore length of, L_p = 0.5354 nm into Dagan's equation,

$$p_Q(R) = \frac{\pi R^4}{\mu(3\pi R + 8L_p)} \tag{8}$$

Hydrodynamics through ultrathin hydrophilic membranes, such as porous nanocrystalline silicon (Pnc-si) membranes, have been shown to be in good agreement with Dagan's equation.[13] Enhancement of volumetric flow rate over no-slip hydrodynamics (eqn (8)) approximately ranges from a factor of three to five for R = 0.5 nm ~ 2 nm. This enhancement over no-slip hydrodynamics is due to the slip at the surface representing advantages of hydrophobic surface of graphene pore.

Additionally, we also estimated the permeation coefficient using the collective diffusion theory[40] (see ESI† for details). Collective diffusion theory assumes that water molecules are

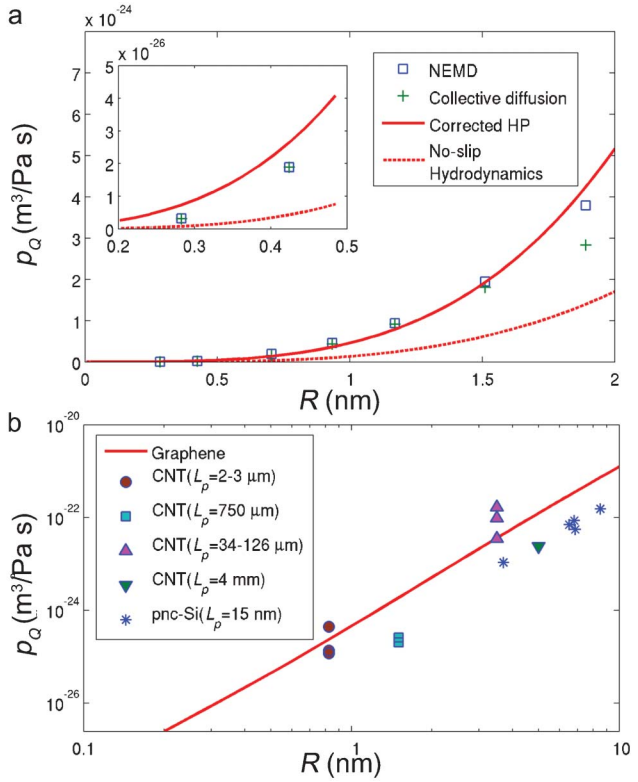

Fig. 6 (a) Permeation coefficients of graphene membranes from NEMD simulations are compared to the theoretical predictions by collective diffusion,[40] corrected HP equation (this work) and no-slip hydrodynamics.[28] Corrected HP relation describes permeation coefficient very well for $R > 0.5$ nm. (b) Theoretically predicted permeation coefficient of graphene membranes by corrected HP relation is compared to the experimental data of CNT membranes[8,9,41,42] and silicon membranes.[13] Some of experimental data reported the permeability based on the membrane area.[9,13,42] *i.e.*, $p_Q = Q_{total}/(\Delta P \cdot A_m)$ where Q_{total} is the total water flow rate through the membrane and A_m is the membrane area. For direct comparison, these experimental data are converted to p_Q as defined in our study (volumetric water flow per pore/total applied pressure).

highly correlated and collectively diffuse through the pore by a chemical potential gradient. In graphene nanopores, when the radius is smaller than 0.484 nm, the collective diffusion theory gives better approximation compared to the corrected HP relation (see inset of Fig. 6(a)). In such small nanopores, single-file water molecules[7,26] are observed and water–water correlation is an important factor for water transport. However, corrected HP relation gives better agreement compared to the collective diffusion theory as the pore radius increases. This indicates that the water transport mechanism transitions from collective diffusion to frictional flow described by the corrected HP relation. Since the corrected HP equation represents the water permeability of graphene nanopores reasonably well, we compare these results to the experimental data of CNT and ultrathin silicon membrane in the next section.

3.6 Comparison of permeability of graphene to CNT and silicon membranes

Assuming that the expressions presented above for the permeation coefficient of graphene nanopores are also valid when the pore radius is larger than 2 nm, we compare the permeability of graphene membranes to the reported values on CNT-based membranes[8,9,41,42] and ultrathin silicon-based membranes.[13] Various experimental data are compared in Fig. 6(b). The CNT membranes are fabricated with lengths ranging from micrometers to millimeters. Silicon-based membranes are fabricated as thin as 15 nm.

Water permeability of the graphene membrane is either comparable or higher than that of a CNT, depending on pore radius or length. Due to the large variation in experimental data of the CNT for $R = 0.83$ nm and $R = 3.5$ nm, it is unclear whether permeability of graphene is higher than that of the CNT. For $R = 1.5$ nm and $R = 5$ nm, CNT length is relatively long and permeability of the graphene membrane is eight-fold and five-fold higher compared to that of the CNT, respectively. We also compared the permeability of the graphene membrane to that of the nanometer-thin Pnc-si membranes[13] in Fig. 6(b). Pnc-si membranes also have high permeability compared to the commercial ultrafiltration membranes or other types of membranes[13] since the nanometer-thin membrane length reduces frictional losses. Permeability of the graphene membrane is approximately four to six-fold higher compared to that of the Pnc-si membrane. Hydrophobic nature of the graphene surface as well as shorter membrane length contributes to the enhanced permeability of the graphene membrane over the hydrophilic Pnc-si membranes.[13]

4. Conclusions

Hydrodynamics through graphene nanopores can be different from nanopores in thicker or longer membranes. Due to the nanometer dimension of the pore, Reynolds number for pressure-driven water flow through graphene nanopores is very small and a linear relation between flow rate and applied pressure drop is observed. Hydrodynamic membrane length is introduced to effectively capture entrance and exit pressure losses. Hydrodynamic membrane length is independent of the applied pressure gradient or fluid velocity, but varies linearly with the pore radius. Water viscosity and slip length decrease with the increase in pore radius due to the water layering effect in the flow direction. Velocity profile and permeation coefficient obtained with the corrected HP equation are found to be in good agreement with molecular simulations. For the small radius pore, where water–water correlation is important, collective diffusion mechanism predicts permeability of graphene quite well. Depending on the pore radius or length, permeability of the graphene nanopore can be either comparable or higher than that of a micrometer-thick CNT membrane. In addition, the permeation coefficient of the graphene nanopore is four to six-fold higher compared to that of nanometer-thick silicon membranes, suggesting that the

graphene membrane is a promising candidate for various applications.

Acknowledgements

This research is supported by NSF under grants 0852657 and 0915718.

References

1 C. Dekker, *Nat. Nanotechnol.*, 2007, **2**, 209–215.
2 M. A. Shannon, P. W. Bohn, M. Elimelech, J. G. Georgiadis, B. J. Marinãs and A. M. Mayes, *Nature*, 2008, **452**, 301–310.
3 T. Hillie and M. Hlophe, *Nat. Nanotechnol.*, 2007, **2**, 663–664.
4 N. Armaroli and V. Balzani, *Angew. Chem., Int. Ed.*, 2007, **46**, 52.
5 B. M. Venkatesan and R. Bashir, *Nat. Nanotechnol.*, 2011, **6**, 615–624.
6 N. W. Ockwig and T. M. Nenoff, *Chem. Rev.*, 2007, **107**, 4078–4110.
7 G. Hummer, J. C. Rasaiah and J. P. Noworyta, *Nature*, 2001, **414**, 188–190.
8 J. K. Holt, H. G. Park, Y. Wang, M. Stadermann, A. B. Artyukhin, C. P. Grigoropoulos, A. Noy and O. Bakajin, *Science*, 2006, **312**, 1034.
9 M. Majumder, N. Chopra, R. Andrews and B. J. Hinds, *Nature*, 2005, **438**, 44.
10 S. Joseph and N. R. Aluru, *Nano Lett.*, 2008, **8**, 452–458.
11 J. A. Thomas and A. J. H. McGaughey, *Nano Lett.*, 2008, **8**, 2788–2793.
12 C. C. Striemer, T. R. Gaborski, J. L. McGrath and P. M. Fauchet, *Nature*, 2007, **445**, 749–753.
13 T. R. Gaborski, J. L. Snyder, C. C. Striemer, D. Z. Fang, M. Hoffman, P. M. Fauchet and J. L. McGrath, *ACS Nano*, 2010, **4**, 6973–6981.
14 M. D. Fischbein and M. Drndi, *Appl. Phys. Lett.*, 2008, **93**, 113107.
15 C. A. Merchant, K. Healy, M. Wanunu, V. Ray, N. Peterman, J. Bartel, M. D. Fischbein, K. Venta, L. U. O. Zhengtang and A. T. Charlie Johnson, *Nano Lett.*, 2010, **10**, 2915–2921.
16 G. F. Schneider, S. W. Kowalczyk, V. E. Calado, G. Pandraud, H. W. Zandbergen, L. M. K. Vandersypen and C. Dekker, *Nano Lett.*, 2010, **10**, 3163–3167.
17 S. Garaj, W. Hubbard, A. Reina, J. Kong, D. Branton and J. A. Golovchenko, *Nature*, 2010, **467**, 190–193.
18 K. Sint, B. Wang and P. Král, *J. Am. Chem. Soc.*, 2008, **130**, 16448–16449.
19 D. E. Jiang, V. R. Cooper and D. A. I. Sheng, *Nano Lett.*, 2009, **9**, 4019–4024.
20 V. P. Sokhan, D. Nicholson and N. Quirke, *J. Chem. Phys.*, 2001, **115**, 3878–3887.
21 G. Cicero, J. C. Grossman, E. Schwegler, F. Gygi and G. Galli, *J. Am. Chem. Soc.*, 2008, **130**, 1871–1878.
22 G. Chen, Y. Guo, N. Karasawa and W. A. Goddard III, *Phys. Rev. B: Condens. Matter*, 1993, **48**, 13959.
23 H. J. C. Berendsen, J. R. Grigera and T. P. Straatsma, *J. Phys. Chem.*, 1987, **91**, 6269–6271.
24 D. Cohen-Tanugi and J. C. Grossman, *Nano Lett.*, 2012, **12**, 3602–3608.
25 F. Zhu, E. Tajkhorshid and K. Schulten, *Biophys. J.*, 2002, **83**, 154–160.
26 M. E. Suk and N. R. Aluru, *J. Phys. Chem. Lett.*, 2010, **1**, 1590–1594.
27 B. Hess, C. Kutzner, D. van der Spoel and E. Lindahl, *J. Chem. Theory Comput.*, 2008, **4**, 435–447.
28 Z. Dagan, S. Weinbaum and R. Pfeffer, *J. Fluid Mech.*, 1982, **115**, 505–523.
29 R. A. Sampson, *Philos. Trans. R. Soc. London, Ser. A*, 1891, **182**, 449–518.
30 J. Happel and H. Brenner, *Low Reynolds Number Hydrodynamics: With Special Applications To Particulate Media*, Kluwer Academic, Hingham, 1991.
31 R. C. Weast, *CRC Handbook of Chemistry and Physics*, CRC Press, Boca Raton, 1986.
32 M. Cieplak, J. Koplik and J. R. Banavar, *Phys. Rev. Lett.*, 2001, **86**, 803–806.
33 J. S. Babu and S. P. Sathian, *J. Chem. Phys.*, 2011, **134**, 4509.
34 H. Zhang, H. Ye, Y. Zheng and Z. Zhang, *Microfluid. Nanofluid.*, 2011, **10**, 403–414.
35 J. H. Walther, T. Werder, R. L. Jaffe and P. Koumoutsakos, *Phys. Rev. E: Stat., Nonlinear, Soft Matter Phys.*, 2004, **69**, 062201.
36 X. Chen, G. Cao, A. Han, V. K. Punyamurtula, L. Liu, P. J. Culligan, T. Kim and Y. Qiao, *Nano Lett.*, 2008, **8**, 2988–2992.
37 T.-D. Li, J. Gao, R. Szoszkiewicz, U. Landman and E. Riedo, *Phys. Rev. B: Condens. Matter Mater. Phys.*, 2007, **75**, 115415.
38 U. Raviv, S. Giasson, J. Frey and J. Klein, *J. Phys.: Condens. Matter*, 2002, **14**, 9275.
39 R. J. Mashl, S. Joseph, N. R. Aluru and E. Jakobsson, *Nano Lett.*, 2003, **3**, 589–592.
40 F. Zhu, E. Tajkhorshid and K. Schulten, *Phys. Rev. Lett.*, 2004, **93**, 224501.
41 F. Du, L. Qu, Z. Xia, L. Feng and L. Dai, *Langmuir*, 2011, **27**, 8437–8443.
42 M. Yu, H. H. Funke, J. L. Falconer and R. D. Noble, *Nano Lett.*, 2008, **9**, 225–229.

